the play vanishes. Hence, from a physical point of view, there is no question of any discrepancy.

Finally, we note that real springboards are tapered from the fulcrum toward the ends, whereas we have assumed that the board has a uniform cross-section. However, by inspection we find that the results obtained here still hold if we use for α_t the harmonic mean $\bar{\alpha}_t$ of the torsional stiffness, i.e.,

$$\bar{\alpha}_t = \frac{1}{\frac{1}{2l}\int_0^{2l} \frac{dx}{\alpha_t(x)}}. \tag{18}$$

Apart from that, it is easy to see that for tapered boards the error resulting from the neglect of the anticlastic bending in this paper will be smaller than for boards with a uniform cross-section. Also, for boards consisting of a plate provided with separate longitudinal stiffeners, the effect of the anticlastic bending is small. However, in the latter case the deformation of the cross-section in its plane will come into play.

Acknowledgment

The authors gratefully acknowledge the stimulating discussions with Prof. Dr. D. J. Gerritsen on the optimal design of springboards. The present problem emerged from these talks.

Slewing Motion Control of a Very Flexible Elastic Beam

J. W. Eischen[12,13], L. Silverberg[12,13], and H. L. Wang[13]

1 Introduction

This Note presents a novel approach to the slewing of beams that are permitted to undergo large combined rigid-body/elastic motions. The problem addressed is a classical noncollocated beam control problem in which a slewing torque is applied at the beam root and sensor measurements are taken at the beam root and the beam tip. Cannon and Schmitz (1984) proposed one of the first feedback control algorithms for such a problem, and as well provided experimental verification. Juang, Turner, and Chun (1985) developed closed-form expressions for control gains that resulted in fuel optimal slewing. Skaar and Tucker (1987) developed classical open-loop and closed-loop control strategies making use of transfer functions. Bayo (1987) employed a structural finite element technique to solve the inverse dynamics problem (open-loop control) for a slewing beam. In each of these investigations, beam motions were restricted to small elastic deflections.

In contrast, this Note presents a strategy well suited for beams undergoing large elastic motions described by nonlinear partial differential equations of motion. The associated torque is governed by a slewing control algorithm consisting of open-loop and closed-loop components. The open-loop component produces the desired overall rigid-body motion of the beam, while the closed-loop component suppresses the elastic vibrational motion relative to a shadow beam. The shadow beam is a fictitious beam whose motion is prescribed by the designer. This concept of a shadow structure was developed by Silverberg and Foster (1990) for maneuvering flexible spacecraft. In the present work, the shadow beam is essentially a straight line that remains tangent to the beam at its root. The closed-loop control component is expressed as a function of three parameters; the collocation gain, the angular displacement gain, and the angular rate gain. The angular displacement gain provides the beam with artificial stiffness and the angular rate gain provides the beam with artificial damping as described by Silverberg and Morton (1989) for this class of structures. The collocation gain provides torque smoothing as well as a means of controlling the degree of sensor/actuator collocation.

The approach introduced in this Note has the potential to apply to a broad class of nonlinear control problems. In view of this, Section 2 reviews general nonlinear beam kinematics. The slewing control algorithm is developed in Section 3. Then Section 4 discusses the efficient numerical integration of the associated equations of motion by an enhanced Newmark (1959) algorithm. Finally, Section 5 presents simulation results.

2 Beam Kinematics

Consider a very flexible beam, subject to a slewing torque applied through a hinge point at the root (see Fig. 1). The beam undergoes arbitrarily large elastic bending, axial, and transverse shear deformations. All motions occur in the horizontal plane absent gravitational effects. No restriction is placed on the magnitude of displacement of points along the elastic axis or on cross-section rotations. Figure 1 shows the flexible beam in an intermediate configuration as well as the associated shadow beam. The angle of rotation of the cross-section at the root is denoted θ_1. This angle defines the orientation of the shadow beam. The inertial displacement components at the beam tip are designated by u_1 and u_2. Longitudinal and transverse displacements at the beam tip relative to the shadow beam are designated by u and v. The connecting angle θ defines the orientation of the line joining the beam root and beam tip. The unstretched length of the beam is L.

The tip displacements relative to the shadow beam are expressed in terms of u_1, u_2, θ_1, and L as follows:

$$-u = [-u_1 - L(1-\cos\theta_1)]\cos\theta_1 - [u_2 - L\sin\theta_1]\sin\theta_1 \tag{1}$$

$$v = [-u_1 - L(1-\cos\theta_1)]\sin\theta_1 + [u_2 - L\sin\theta_1]\cos\theta_1. \tag{2}$$

The time derivatives of u and v are easily expressed in terms of u_1, u_2, $\dot{u}_1$, $\dot{u}_2$, θ_1, and $\dot{\theta}_1$. The connecting angle is simply

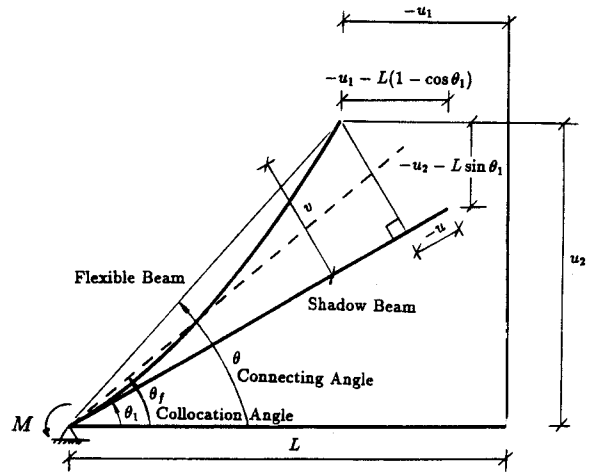

Fig. 1 Geometry and deformation measures for the elastic beam

[12]Mem. ASME.

[13]Department of Mechanical and Aerospace Engineering, North Carolina State University, Raleigh, NC 27695-7910.

Contributed by the Applied Mechanics Division of THE AMERICAN SOCIETY OF MECHANICAL ENGINEERS. Manuscript received by the ASME Applied Mechanics Division, Nov. 20, 1990; final revision, Apr. 30, 1991. Associate Technical Editor: D. J. Inman.

$$\theta = \tan^{-1}\left[\frac{u_2}{L+u_1}\right] \quad \text{for } L+u_1 \geq 0 \tag{3}$$

$$\theta = \pi + \tan^{-1}\left[\frac{u_2}{L+u_1}\right] \quad \text{for } L+u_1 < 0. \tag{4}$$

The time derivative of θ is easily expressed in terms of u_1, u_2, $\dot{u}_1$, and $\dot{u}_2$.

3 Beam Control

The proposed slewing control algorithm is an implicit function of inertial measurements of displacements and velocities at the beam tip: u_1, u_2, $\dot{u}_1$, $\dot{u}_2$, and also makes explicit use of the root angle θ_1, the connecting angle θ and their time derivatives. Furthermore, two additional quantities are introduced to aid in the development of the slewing algorithm. The two quantities are a desired path angle $\theta_0(t)$ and a collocation angle $\theta_f(t)$. The desired path angle is expressed in the polynomial form

$$\theta_0(t) = a_0 + a_1 t + a_2 t^2 + a_3 t^3 + a_4 t^4 + a_5 t^5 \quad t \leq T \tag{5}$$

where T is the slewing time. The coefficients a_0 through a_5 are determined by appropriate initial and final states. In the numerical example presented here, the beam is slewed 90 deg counterclockwise in a rest-to-rest maneuver. The initial and final states are

$$\theta_0(0) = 0 \quad \dot{\theta}_0(0) = 0 \quad \ddot{\theta}_0(0) = 0 \tag{6}$$

$$\theta_0(T) = \frac{\pi}{2} \quad \dot{\theta}_0(T) = 0 \quad \ddot{\theta}_0(T) = 0. \tag{7}$$

For a slewing time $T = 5$, the coefficients for $t \leq T$ are

$$a_0 = a_1 = a_2 = 0,\ a_3 = 0.12566371,$$
$$a_4 = -0.03769911,\ a_5 = 0.00301593 \tag{8}$$

and for $t > T$ are

$$a_0 = \frac{\pi}{2},\ a_1 = a_2 = a_3 = a_4 = a_5 = 0. \tag{9}$$

The slewing torque is expressed as

$$M(t) = M_0(t) + M_c(t) \tag{10}$$

where M_0 represents an open-loop torque and M_c represents a closed-loop torque. The open-loop torque controls gross overall slewing motion, while the closed-loop torque controls elastic motions relative to the desired nominal path. The open-loop torque M_0 is simply the torque required to maneuver a rigid beam along the desired path. Thus,

$$M_0 = I_m \ddot{\theta}_0 \tag{11}$$

where $I_m = mL^2/3$ is the mass moment of inertia of the rigid beam about the hinge point and m is the total mass of the beam. The closed-loop torque is defined as

$$M_c = -(\alpha_1^2 + \alpha_2^2) I_m (\theta_f - \theta_0) - 2\alpha_1 I_m (\dot{\theta}_f - \dot{\theta}_0) \tag{12}$$

where θ_f represents a collocation angle defined here as

$$\theta_f \equiv \theta_1 + \beta_c(\theta - \theta_1). \tag{13}$$

The parameters α_1, α_2, and β_c are selected by the designer. The parameter α_1 controls damping of the beam motions, α_2 controls the frequency of oscillation, and β_c represents a torque smoothing parameter. The quantity β_c may also be interpreted as a collocation parameter, and enables the introduction of the collocation angle θ_f, as shown in Eq. (13). As β_c varies between 0 and 1, the collocation angle varies continuously between θ_1 and θ. When $\beta_c = 0$, $\theta_f = \theta_1$ and the feedback control is collocated, i.e., the sensor $(\theta_1, \dot{\theta}_1)$ is collocated with the actuator $(M(t))$. If the beam were absolutely rigid, α_1 would be identical to the damping rate, and α_2 would be equal to the closed-loop frequency. When $\beta_c > 0$, then the sensor and actuator are noncollocated, i.e., when $\beta_c = 1$, $\theta_f = \theta$.

4 Dynamic Finite Element Analysis

The slewing motions of very flexible beams under the influence of control torques are governed by nonlinear partial differential equations (PDE's) of motion. The derivation of these PDE's and their efficient numerical solution by a finite element discretization procedure was proposed by Simo and Vu-Quoc (1986). The beam is effectively divided into a series of finite elements, joined at nodal points whose positions are selected by the analyst. The spatially discretized equations of motion for the large deformation beam theory proposed by Simo and Vu-Quoc (1986) are conveniently presented in a form commonly encountered in nonlinear structural dynamics,

$$\mathbf{Ma} + \mathbf{P(d)} = \mathbf{F}^c(\mathbf{d}, \mathbf{v}) \tag{14}$$

where $\mathbf{d}$ is a vector containing nodal displacements and cross-section rotations, $\mathbf{v}$ is a vector containing nodal velocities and cross-section angular velocities, and $\mathbf{a}$ is a vector containing nodal accelerations and cross-section angular accelerations. $\mathbf{M}$ is the symmetric system mass matrix. The mass matrix is time invariant here because kinematic quantities are referred to an inertial reference frame, i.e., there are no rotating reference frames. $\mathbf{P(d)}$ is the nonlinear internal force vector and $\mathbf{F}^c(\mathbf{d}, \mathbf{v})$ is the system control force vector. Details regarding the numerical solution of Eq. (14) in which $\mathbf{F}^c(\mathbf{d}, \mathbf{v}) = \mathbf{0}$ are given in the paper by Simo and Vu-Quoc (1986). The computational procedure developed by Simo and Vu-Quoc (1986) is summarized briefly as follows, along with an extension that incorporates the control force.

Essentially, the computational task is to advance an equilibrium solution from known values of $\mathbf{d}_n$, $\mathbf{v}_n$, and $\mathbf{a}_n$ at time $t = t_n$ to values $\mathbf{d}_{n+1}$, $\mathbf{v}_{n+1}$, and $\mathbf{a}_{n+1}$ at $t = t_{n+1}$. This can be accomplished by combining the Newton-Raphson method for solving nonlinear systems of equations with the Newmark (1959) method for solving second-order systems of ordinary differential equations. The key steps in the solution algorithm are described as:

Displacement/Velocity Predictors:

$$\tilde{\mathbf{d}}_{n+1}^{(i)} = \mathbf{d}_n + \Delta t \mathbf{v}_n + \frac{\Delta t^2}{2}(1-2\beta)\mathbf{a}_n \tag{15}$$

$$\tilde{\mathbf{v}}_{n+1}^{(i)} = \mathbf{v}_n + \Delta t(1-\gamma)\mathbf{a}_n. \tag{16}$$

The superscript $^{(i)}$ is an iteration counter, initially set to 0. Note that $\mathbf{a}_{n+1}^{(0)} = 0$. Newmark parameters are indicated by β and γ. These adjustable parameters control the stability and accuracy of the Newmark algorithm. For this work, $\beta = 1/4$ and $\gamma = 1/2$, corresponding to the trapezoidal rule. The following linear system of algebraic equations is then solved to generate the incremental acceleration $\Delta\mathbf{a}$,

$$\left[\mathbf{M} - \gamma\Delta t \frac{\partial \mathbf{F}^c(\tilde{\mathbf{d}}_{n+1}^{(i)}, \tilde{\mathbf{v}}_{n+1}^{(i)})}{\partial \mathbf{v}} + \beta\Delta t^2 \left(\frac{\partial \mathbf{P}(\tilde{\mathbf{d}}_{n+1}^{(i)})}{\partial \mathbf{d}} - \frac{\partial \mathbf{F}^c(\tilde{\mathbf{d}}_{n+1}^{(i)}, \tilde{\mathbf{v}}_{n+1}^{(i)})}{\partial \mathbf{d}}\right)\right]\Delta\mathbf{a} = \mathbf{F}^c(\tilde{\mathbf{d}}_{n+1}^{(i)}, \tilde{\mathbf{v}}_{n+1}^{(i)}) - \mathbf{P}(\tilde{\mathbf{d}}_{n+1}^{(i)}) \tag{17}$$

or

$$\mathbf{M}^* \Delta\mathbf{a} = \mathbf{R}_{n+1}^{(i)} \tag{18}$$

where $\mathbf{M}^*$ is the effective mass matrix, and $\mathbf{R}_{n+1}^{(i)}$ is referred to as the residual.

Displacement/Velocity/Acceleration Updates: After solving for the acceleration $\Delta\mathbf{a}$ in Eq. (18), calculate

$$\tilde{\mathbf{d}}_{n+1}^{(i+1)} = \tilde{\mathbf{d}}_{n+1}^{(i)} + \beta\Delta t^2 \Delta\mathbf{a} \tag{19}$$

$$\tilde{\mathbf{v}}_{n+1}^{(i+1)} = \tilde{\mathbf{v}}_{n+1}^{(i)} + \gamma\Delta t \Delta\mathbf{a} \tag{20}$$

$$\tilde{\mathbf{a}}_{n+1}^{(i+1)} = \tilde{\mathbf{a}}_{n+1}^{(i)} + \Delta\mathbf{a}. \tag{21}$$

A convergence check is performed at this stage by forming the ratio $\|\mathbf{R}_{n+1}^{(i+1)}\| / \|\mathbf{R}_{n+1}^{(0)}\|$. If this ratio is greater than a pre-

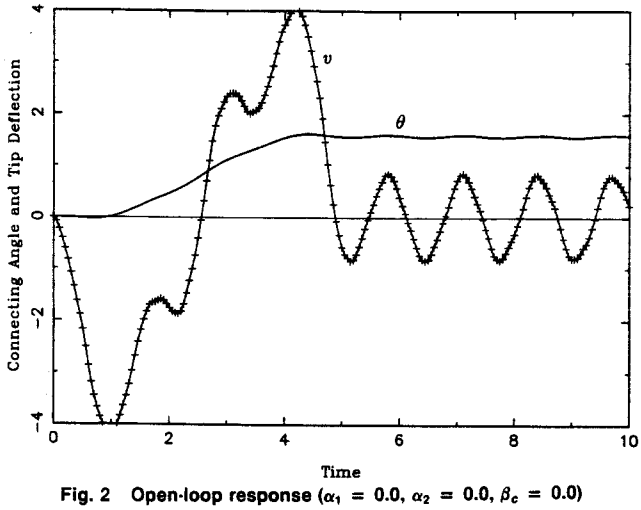

Fig. 2 Open-loop response ($\alpha_1 = 0.0$, $\alpha_2 = 0.0$, $\beta_c = 0.0$)

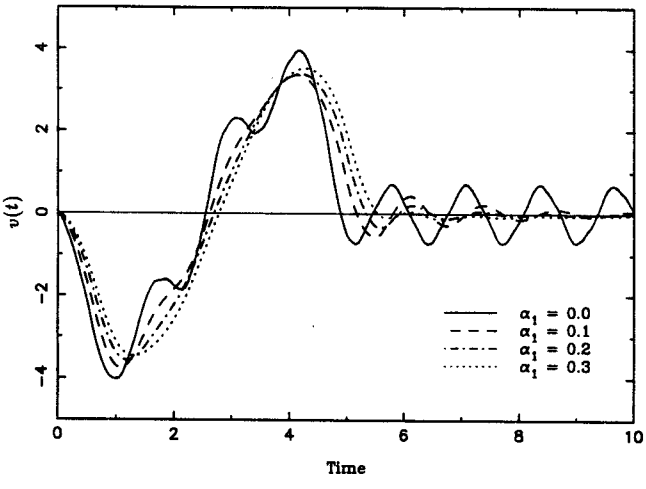

Fig. 3 Closed-loop response sensitivity to control parameter α_1 ($\alpha_2 = 0.2$, $\beta_c = 0.3$)

specified error tolerance, Eq. (18) is solved again using the new updated kinematic quantities. If this ratio is less than the user-specified tolerance (1.0×10^{-8} in our work), convergence is achieved and the desired kinematic quantities at $t = t_{n+1}$ are

$$\mathbf{d}_{n+1} = \tilde{\mathbf{d}}_{n+1}^{(i+1)} \quad \mathbf{v}_{n+1} = \tilde{\mathbf{v}}_{n+1}^{(i+1)} \quad \mathbf{a}_{n+1} = \tilde{\mathbf{a}}_{n+1}^{(i+1)} \tag{22}$$

Explicit expressions for $\mathbf{M}$, $\mathbf{P}$, and $\partial \mathbf{P}/\partial \mathbf{d}$ (tangent stiffness) are contained in the paper by Simo and Vu-Quoc (1986). The term $\partial \mathbf{F}^c/\partial \mathbf{d}$ involves derivatives of the control moment with respect to certain finite element nodal kinematical quantities. In the present control algorithm, these quantities are the cross-section rotation and angular velocity at the hinge point and the inertial displacements and velocities at the beam tip. The partial derivatives $\partial M/\partial \theta_1$, $\partial M/\partial u_1$, $\partial M/\partial u_2$ are calculated and added properly to the $\mathbf{M}^*$ matrix above. These quantities clearly depend on $\partial \theta/\partial u_1$, $\partial \theta/\partial u_2$, $\partial \dot{\theta}/\partial u_1$, and $\partial \dot{\theta}/\partial u_2$, which are calculated from Eq. (3). Likewise, the tangent damping matrix $\partial \mathbf{F}^c/\partial \mathbf{v}$ involves the derivatives $\partial M/\partial \dot{\theta}_1$, $\partial M/\partial \dot{u}_1$, $\partial M/\partial \dot{u}_2$, which in turn depend on $\partial \dot{\theta}/\partial \dot{u}_1$ and $\partial \dot{\theta}/\partial \dot{u}_2$.

5 Simulation Results

The flexible beam is discretized with ten finite elements. The following physical parameters were selected:

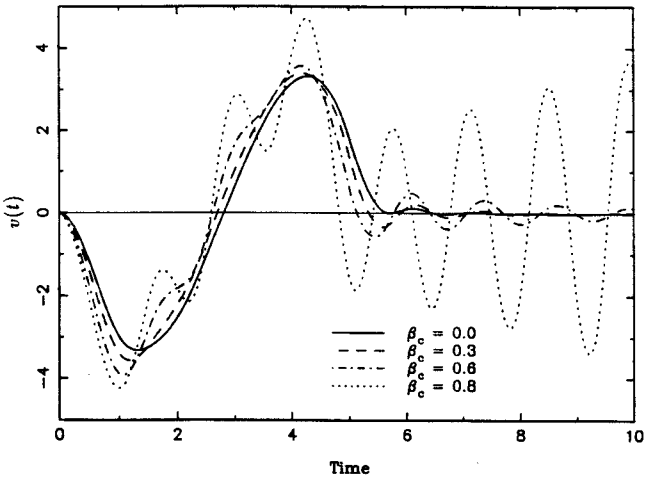

Fig. 4 Closed-loop response sensitivity to control parameter β_c ($\alpha_1 = 0.2$, $\alpha_2 = 0.2$)

$L = 10$ (total length)

$E = 10{,}000$ (elastic modulus)

$G = 12{,}000$ (shear modulus)

$A = 1$ (cross-sectional area)

$I = 1/10$ (second moment of area)

$\rho = 1$ (mass density).

Figure 2 shows the response of the connecting angle θ and the tip deflection v for open-loop control ($\alpha_1 = \alpha_2 = 0$). In the case of open-loop control, the connecting angle θ is identical to the desired path angle θ_0 if the beam is rigid. Since the simulations performed here are representative of a very flexible beam, oscillations associated with the fundamental bending vibration mode are detected, and after the maneuver period ($T = 5$), the connecting angle oscillates about the desired value $\theta_0 = \pi/2$. The tip deflection oscillates about zero with no damping. Note the very large transverse bending deflections of ± 4 compared to the beam length $L = 10$. This and subsequent simulations use an integration time step $\Delta t = 0.5$. The fundamental period T_f for the bending mode calculated from classical linear vibration theory (pinned-free beam) is $T_f = 2\pi/(3.926602)^2 \ (EI/\rho AL^4)^{-1/2} = 1.289$. The simulation agrees well with this result.

Figure 3 shows the tip deflection response for the case $\alpha_2 = 0.2$ and $\beta_c = 0.3$. For $0 \le \alpha_1 \le 0.3$, the response is clearly stable, and the elastic motion of the beam is slowly damped in time. As the control parameter α_1 increases, the damping rate increases. For $\alpha_1 = 0.3$, the elastic motions are suppressed after a few oscillations beyond the maneuver time $T = 5$. Figure 4 shows the time response of the tip deflection $v(t)$ as a function of the parameter β_c, holding α_1 and α_2 constant. This figure highlights the effect of the noncollocated control on the response in the presence of altered stiffness characteristics. Figure 5 shows the region of stability corresponding to the physical parameters listed above. Instability arises as the collocation parameter increases beyond critical levels. Figure 6 shows the fuel consumption F_{ul} defined by $F_{ul} = \int_0^\infty |M| dt$ for a range of values of the parameters α_1 and β_c, holding $\alpha_2 = 0$. It is significant to note that the fuel consumption is maximum for collocated control ($\beta_c = 0$), and decreases as the collocation parameter increases.

6 Conclusions

A simple method has been proposed to control the slewing motion of a very flexible elastic beam. The control system

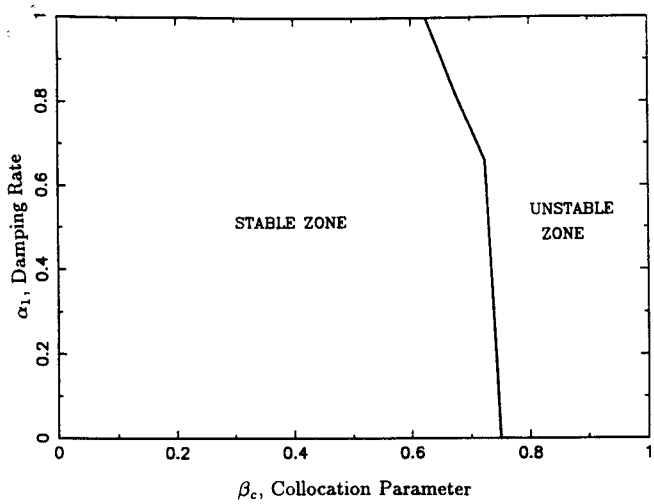

Fig. 5 Control system stability plot

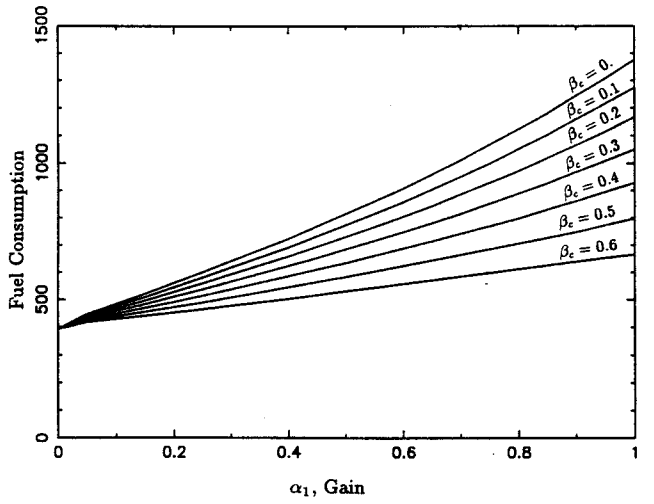

Fig. 6 Fuel consumption versus α_1 and β_c (α_2 = 0.0)

relies on sensing position and velocity information at the beam tip together with angular position and rate at the beam root. Simulations demonstrate that the control system performs very well for a large angle slewing maneuver for a beam that experiences large elastic bending deformations. Furthermore, it is shown how the fuel consumption decreases as the sensors become noncollocated with the actuators.

References

Bayo, E., 1987, "A Finite Element Approach to Control the End-Point Motion of a Single-Link Flexible Robot," *Journal of Robotic Systems*, Vol. 4, No. 1, pp. 63-75.

Cannon, R. H., and Schmitz, E., 1984, "Initial Experiments on the End-Point Control of a Flexible One-Link Robot," *The International Journal of Robotics Research*, Vol. 3, No. 3, pp. 62-75.

Juang, J. N., Turner, J. D., and Chun, H. M., 1985, "Closed-Form Solutions of Control Gains for a Terminal Controller," *Journal of Guidance, Control, and Dynamics*, Vol. 8, pp. 38-43.

Newmark, N. M., 1959, "A Method of Computation for Structural Dynamics," *ASCE Journal of the Engineering Mechanics Division*, pp. 67-94.

Simo, J. C., and Vu-Quoc, L., 1986, "On the Dynamics of Flexible Beams Under Large Overall Motions—The Plane Case: Parts I and II," ASME JOURNAL OF APPLIED MECHANICS, Vol. 53, No. 4, pp. 849-863.

Skaar, S. B., and Tucker, D., 1986, "Point Control of a One-Link Flexible Manipulator," ASME JOURNAL OF APPLIED MECHANICS, Vol. 53, pp. 23-27.

Silverberg, L., and Foster, L. A., 1990, "Decentralized Feedback Maneuver of Flexible Spacecraft," *Journal of Guidance, Control, and Dynamics*, Vol. 13, No. 2, pp. 258-264.

Silverberg, L., and Morton, M., 1989, "On the Nature of Natural Control," *Journal of Vibration, Stress, and Reliability in Design*, Vol. 111, pp. 412-422.

Absence of One Nodal Diameter Critical Speed Modes in an Axisymmetric Rotating Disk

Anthony A. Renshaw,[14,16] and C. D. Mote, Jr.[15,16]

Introduction

Numerically computed eigenvalues of an axisymmetric, rotating disk suggest that the natural vibration frequencies with one nodal diameter are bounded below by the rotation frequency of the disk. This Brief Note proves the existence of this bound for a large class of axisymmetric stress fields and boundary conditions.

The bound bears directly on the critical speed instability of rotating disks. The critical speed of a rotating disk is the lowest rotation speed at which the propagation speed of a backward traveling circumferential wave equals the rotation speed. At critical speed the propagating wave is stationary in the nonrotating reference frame and is excited to resonance by a stationary, transverse force. Since the 1920's, both numerical and experimental results on centrally clamped, spinning disks have never found a critical speed mode with zero or one nodal diameters (e.g., Lamb and Southwell, 1921; Southwell, 1922; Tobias and Arnold, 1957; Mote, 1970; Iwan and Moeller, 1976). The zero nodal diameter mode can be critical only if its eigenvalue is zero; this is not possible if the Rayleigh Quotient is positive definite. The one nodal diameter mode, however, is critical when its eigenfrequency equals the rotation frequency. Although previous studies noted the absence of one nodal diameter critical speed modes for their specific cases, no general conditions under which this would occur were set forth.

The proof that one nodal diameter natural frequencies are bounded by the rotation frequency rests on two observations. First, equilibrium under a centripetally induced stress field ensures that the completely free rotating disk has an eigenfunction whose eigenfrequency exactly equals the rotation frequency. This eigenfunction corresponds to rigid-body tilting of the disk about the nodal diameter. Second, although the method of multiplicative variation is typically useful only for nonvanishing eigenfunctions (Courant and Hilbert, 1957), it can be used with one nodal diameter eigenfunctions provided that the stresses and boundary conditions are axisymmetric. If the vibration problem is asymmetric, then the nodal lines of the resulting vibration modes cannot be predicted in advance and the proof is not valid.

Eigenvalue Problem and Stress Field

Eigensolutions for the transverse displacement of a uniform, axisymmetric disk satisfy the self-adjoint, dimensionless equation

$$\nabla^4 w - \frac{1}{r}(r\sigma_r w_{,r})_{,r} - \frac{1}{r^2}\sigma_\theta w_{,\theta\theta} = \lambda^2 w \qquad (1)$$

plus appropriate boundary conditions, where $w(r,\theta)$ is the transverse displacement, σ_r and σ_θ are the radial and hoop stresses, ∇^4 is the biharmonic operator, a comma denotes partial differentiation, λ^2 is the eigenvalue, and λ is the natural frequency. Solutions to (1) render the Rayleigh Quotient, J, stationary with $J = \lambda^2$:

[14]Graduate Student.

[15]FANUC Chair in Mechanical Systems and Vice Chancellor. Fellow ASME.

[16]Department of Mechanical Engineering, University of California, Berkeley, CA 94720.

Contributed by the Applied Mechanics Division of THE AMERICAN SOCIETY OF MECHANICAL ENGINEERS. Manuscript received by the ASME Applied Mechanics Division, Dec. 18, 1990; final revision, Apr. 2, 1991. Associate Technical Editor: D. J. Inman.